Journal of Applied Electrochemistry **32**: 73–83, 2002.

Influence of heat transfer on anodic oxidation of aluminium

I. DE GRAEVE[1], H. TERRYN[1] and G.E. THOMPSON[2]
[1]*University of Brussels, Department of Metallurgy, Electrochemistry and Materials Science, Brussels, Belgium*
[2]*University of Manchester Institute of Science and Technology, Corrosion and Protection Centre, Manchester, Great Britain*

Received 15 January 2001; accepted in revised form 2 October 2001

Key words: anodizing, heat transfer, oxide distribution, wall-jet electrode

Abstract

The influence of convective heat transfer on constant current density anodizing of aluminium in sulfuric acid has been examined in a wall-jet electrode reactor. The uniformity of the anodic film thickness is related to the local electrode temperature distribution, which is dependent on the convection. The higher the local temperature, the greater the local oxide thickness. An increased local temperature enhances local field assisted oxide dissolution at the pore bases, and consequently acts to increase the local current density. At relatively high current densities, local features develop on the electrode surface, accompanied by high initial, local temperature rises. The relevance of such local features, limiting useful oxide growth, is considered further.

1. Introduction

Anodizing is employed routinely to form compact- or porous-type oxide films on aluminium for diverse applications ranging from electrolytic capacitors to protective coatings [1]. The anodic oxide thickness increases with the charge passed (i.e., the product of current density and time), whereas the oxide morphology and composition depend on the specific anodizing conditions [1, 2]. The oxide growth mechanism is based on high-field ionic migration [3, 4], with field strengths of 10^8–10^9 V m^{-1} necessary to sustain ionic transport.

The nature of the mobile species and the mechanisms of transport through the anodic film have received attention [3–6]. In acid electrolytes (e.g., sulfuric, phosphoric and oxalic acids) aluminium is oxidized and forms solid oxide at the metal–film interface by O^{2-} ingress across the preexisting oxide film; simultaneous Al^{3+} egress leads to cation ejection at the film–electrolyte interface [2]. The latter results in initial nonuniform film thickening, concentration of the electric field in thin film regions and the onset of field assisted dissolution [7–11], which proceeds in dynamic equilibrium with film growth during the steady region of anodizing.

The steady-state anodic film comprises an outer porous region above a relatively compact barrier layer. Cylindrical pores are located at the centres of cells and pass perpendicularly to the substrate surface [1]. They are separated from the substrate by the barrier layer with its hemispherical appearance.

On the one hand, for some anodizing conditions, particularly high current densities and/or high electrolyte temperatures, local burning [12–15] of the aluminium and/or poor uniformity of the anodic film (e.g., oxide thickness distribution over the aluminium surface) occur. Precise reasons for such behaviour are awaited, but a primary cause can often be traced to the hydrodynamic flow pattern of the electrolyte during anodizing. Electrolyte agitation or convection is largely responsible for mass and heat transfer in the treatment bath during the electrochemical process. Diggle [4] has considered the possible rate determining steps for oxide formation based on high-field ionic migration; mass transfer in the solution does not determine the rate of the reaction.

On the other hand, unlike many other electrochemical processes, significant heat is produced during anodizing. Estimates [16–18], calculations [19] or measurements [14, 20–25] have indicated that the aluminium and the adjacent electrolyte can reach temperatures considerably higher than the bulk electrolyte temperature during anodizing. The three main heat sources are exothermic heat liberated during oxide growth, Joule heating of the electrolyte and, most importantly, Joule heating of the oxide covered aluminium due to the high oxide resistance. Such heat is dissipated by thermal conduction in the aluminium and the solution and, more effectively, by electrolyte convection during the process. It is at this point where convection becomes important for anodizing and more specifically, the convective heat transfer. Tu [14] has considered effects of stirring the electrolyte during oxalic acid anodizing. Effective heat removal impacted on reduced thermal enhancement of the field assisted dissolution, resulting in an increased anodizing

voltage and increased barrier layer thickness. A further benefit was the increased overall oxide layer thickness, due to reduced chemical dissolution of the film, contributing to film friability. Pierrard [23] revealed similar effects for anodizing in phosphoric acid.

The present authors have revealed that during d.c.-anodizing in sulfuric acid, the anodic oxide thickness is not uniform for certain anodizing conditions, particularly when high current densities are employed. The influence of heat transfer on anodizing, including film uniformity and burning, awaits elucidation. In the present work, the effect of convection during anodizing on a planar surface has been considered as the first step in a systematic study defining electrolyte flow and heat transfer. The effects of heat transfer have been examined with a laboratory scale, wall-jet electrode reactor [26–28]. The major advantage of the wall-jet electrode is the nonuniform accessibility [29], leading to a local heat transfer coefficient distribution (nonuniform thermal boundary layer) over the electrode surface.

2. Experimental details

AA1050 aluminium (99.5% Al sheet, thickness 3 mm) was cut to provide samples of 55 mm diameter; the exposed surface area in the reactor cell was 1260 mm^2 (dia. 40 mm).

Figures 1 and 2 show schematic diagrams of the wall-jet electrode reactor and the wall-jet hydrodynamic flow pattern [26]. A submerged jet, from a circular nozzle (dia. 2 mm), located 26 mm from the centre of the working electrode, impinges perpendicularly to the electrode and spreads out symmetrically in the radial direction. Due to the specific wall-jet hydrodynamics, the convective transfer coefficients are highest at the

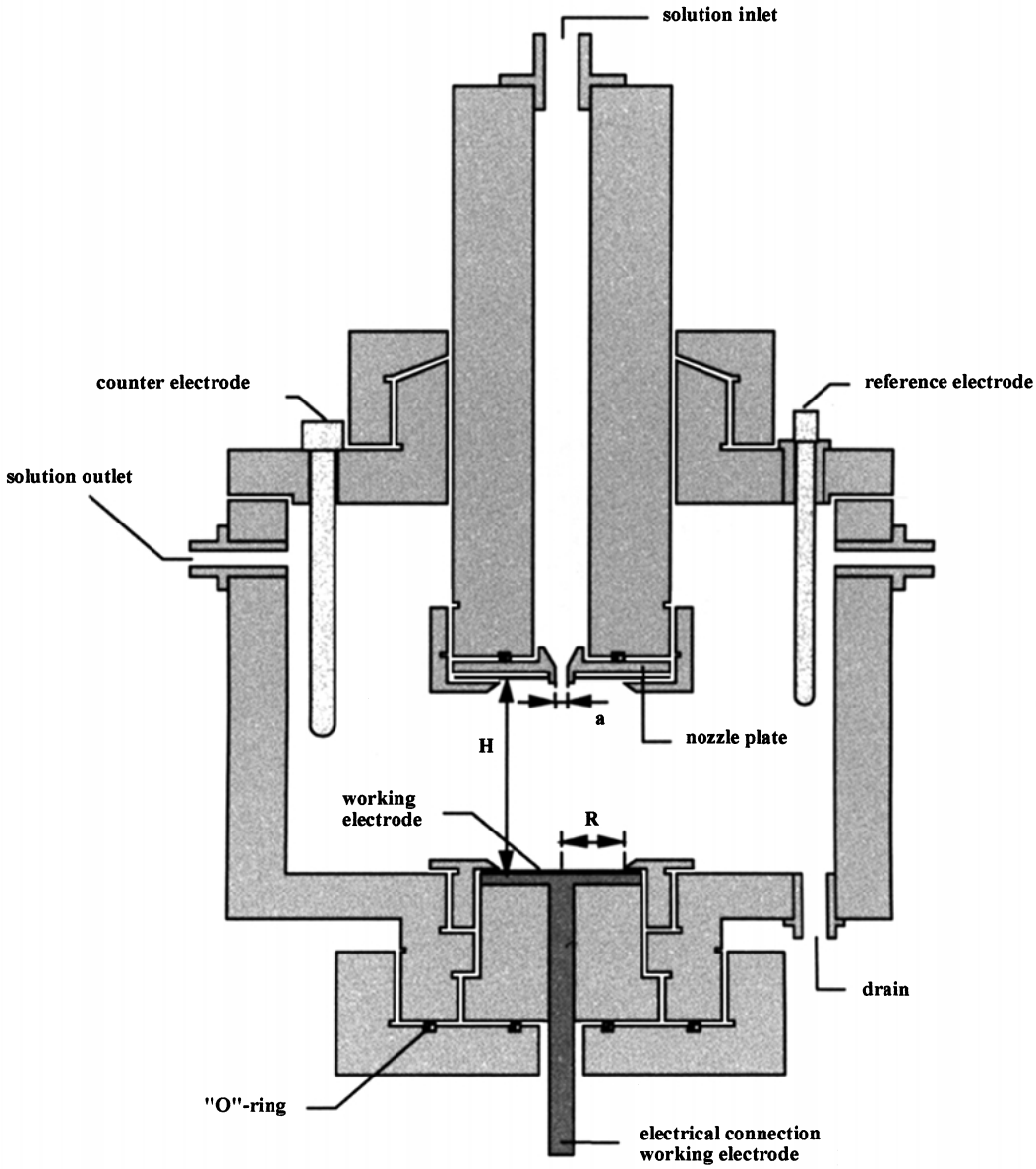

Fig. 1. Schematic diagram of the wall-jet electrode reactor.

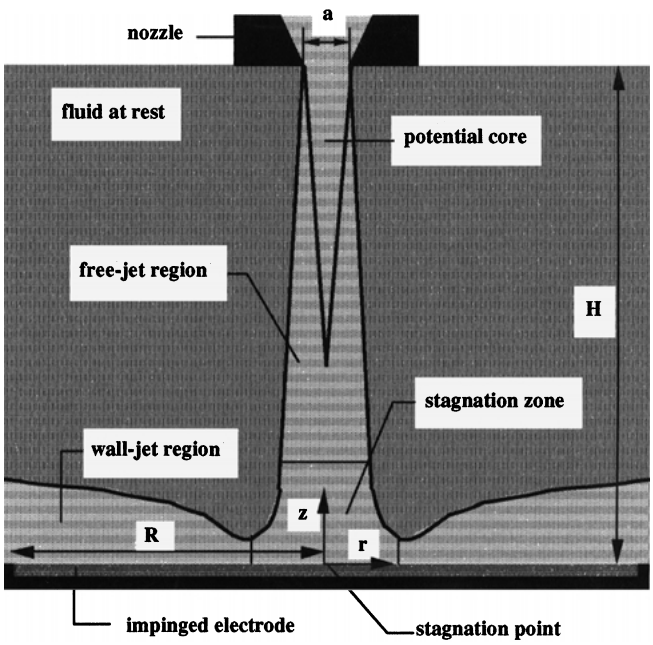

Fig. 2. Schematic diagram of the wall-jet electrode hydrodynamic flow pattern.

centre of the electrode, where fresh electrolyte impinges on the surface, and decline towards the rim of the circular electrode [30–32]. Five embedded thermocouples (type TT) in the sample holder (Figure 3) make direct contact with the back face of the thin aluminium electrode. T1 and T5 are at diametrically opposite positions (±15 mm from centre) and should register similar temperatures, verifying the axial symmetry of the wall-jet hydrodynamics. T3 is positioned at the centre of the electrode, and T2 and T4 are, respectively, +10 and −5 mm from T3. In order to ensure good thermal contact, conducting paste was applied separately to each thermocouple before each experiment.

Three jet conditions have been used throughout the experiments. In the zero jet condition, natural convection due to buoyancy forces prevails. The initially stagnant electrolyte, adjacent to the electrode surface, becomes warmer during anodizing and moves upwards in the cell, thus creating a natural flow pattern with fresh electrolyte being drawn in from the rim of the sample. The forced flow conditions were selected in the valid laminar wall-jet regime and thus obey Figure 2. Flows 1 and 2 have nozzle exit Reynolds numbers of 770 and 1507, respectively.

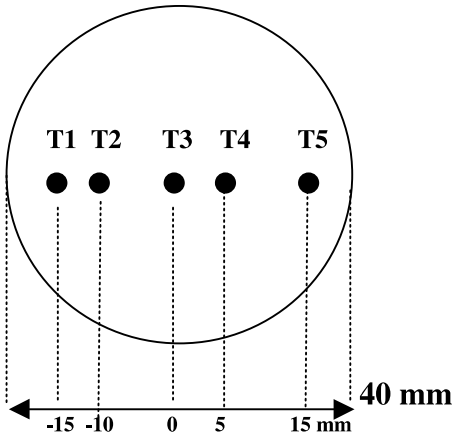

Fig. 3. Top view of the sample holder and the five imbedded thermocouples.

Prior to anodizing, samples were degreased in 2 wt % PARCO 4103/1 at 65–70 °C for 30 s. Anodizing at a constant current density was performed in 20 wt % H_2SO_4 at 25 °C; current densities ranged from 0.8 to 20 A dm^{-2} (8–200 mA cm^{-2}), spanning the conditions used in batch and continuous anodizing applications.

The electrolyte for the reactor cell was thermostatically heated to the desired temperature (±1 °C) in a 30 L reservoir. The required constant current was supplied by an AMEL 555B potentiostat/galvanostat between the working electrode and an aluminium rod counter electrode. The potential response during the process was recorded with a Nicolet 310 oscilloscope between the working electrode and a saturated calomel reference electrode.

The thickness of relatively thin anodic films was determined by X-ray energy dispersive analysis (EDX) combined with scanning electron microscopy (Jeol JSM6400) to an accuracy of ±10 nm [33]. Calibration was undertaken on standard samples of known film thickness, determined previously with ellipsometry and transmission electron microscopy [34]. The ratios of the intensities of oxygen to aluminium (for constant EDX/SEM settings) with film thickness yielded a calibration line for films up to 1 μm thickness.

For films of increased thickness (>5 μm), eddy current measurements were made with a calibrated Fischer Dualscope MP20; measurements were made to an accuracy of ±1 μm.

3. Results

3.1. *Influence of convection on the electrochemical potential response*

Figure 4 shows the variation of potential, after a constant charge density of 80 C dm^{-2} has been passed, with current density and jet flow rate. It is evident that the potential is lower for the zero jet condition than for jet flows 1 and 2, particularly at high current densities.

Potential–time transients are shown in Figures 5 and 6 for anodizing at 4 and 20 A dm^{-2} under different flow conditions. Initial nonuniform film growth and thickening of the barrier layer lead to a rapid potential increase and, with continued anodizing, the transients reveal a steady-state region. The steady-state potential is lower for the zero jet condition compared with forced convection, in agreement with previous findings [23].

At 20 A dm^{-2}, the potentials are higher than at lower current densities, as expected; further, for the zero jet condition, the steady-state potential is approximately constant, whereas the potential increases significantly with time for jet flows 1 and 2.

3.2. *Appearance of the electrodes*

After anodizing, regions of different appearance are revealed in symmetrical patterns on the electrode surface. Samples anodized at 4 A dm^{-2} for 20 s under the zero jet condition show concentric rings of differing appearances. For anodizing at current densities of 8 A dm^{-2} and above, a distinct white spot is present

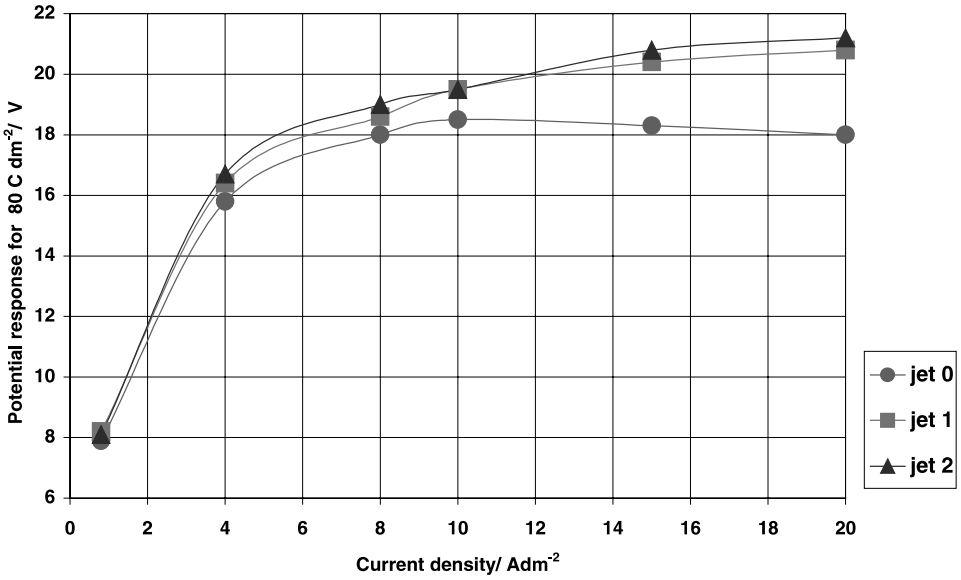

Fig. 4. Variation of the potential with current density and jet flow for anodizing in 20 wt % H_2SO_4 at 25 °C.

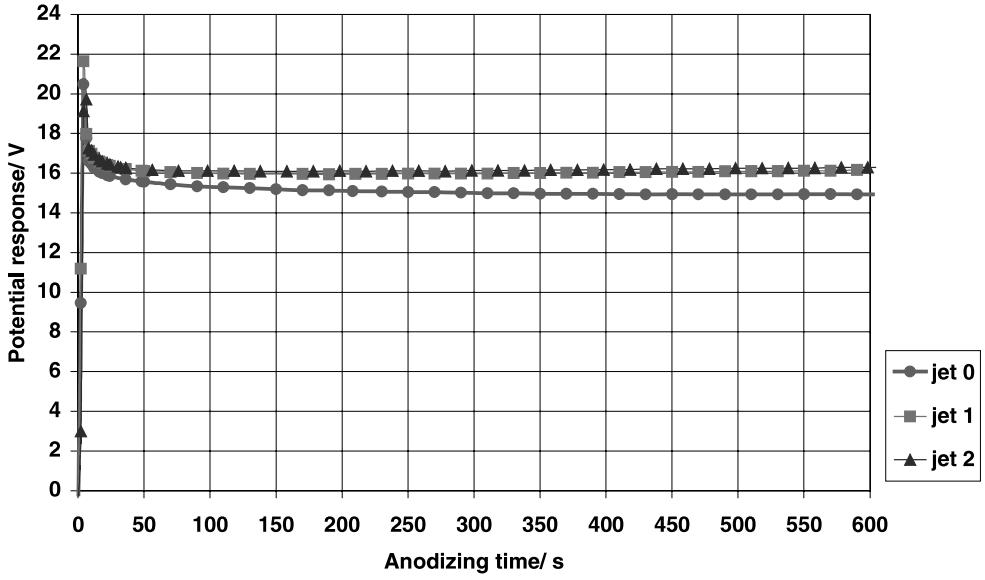

Fig. 5. Potential–time transient for anodizing at current density 4 A dm^{-2} in 20 wt % H_2SO_4 at 25 °C under different jet flow conditions.

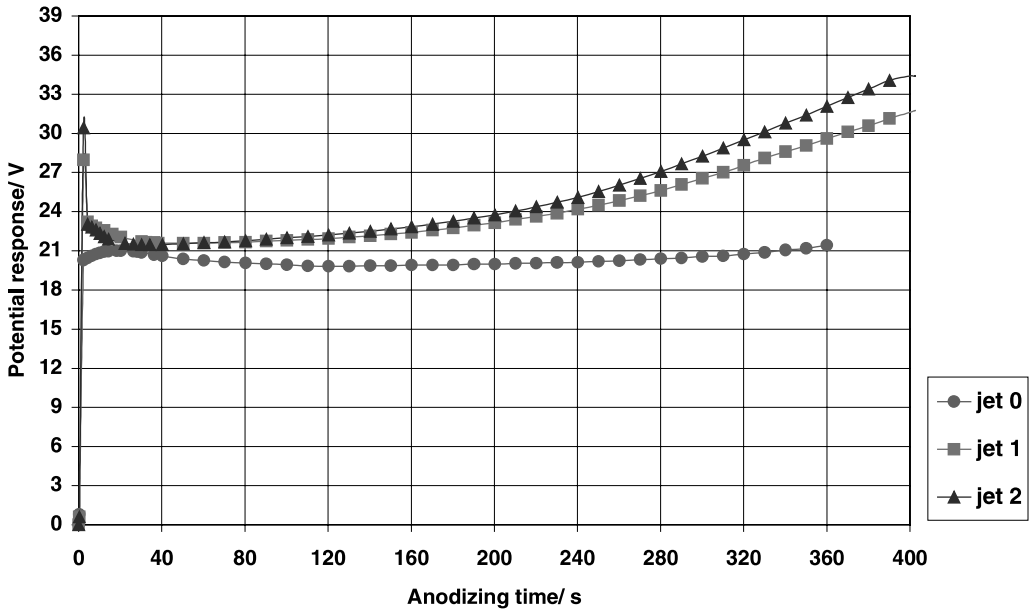

Fig. 6. Potential–time transient for anodizing at current density 20 A dm^{-2} in 20 wt % H_2SO_4 at 25 °C under different jet flow conditions.

on the electrode surface. The spot position varies with jet flow, being located at the centre of the electrode for the zero jet condition and at more eccentric positions with increase in jet flow rate.

3.3. *Influence of convection on the local oxide thickness*

To examine the influence of current density, the oxide thickness was measured after a constant charge passed through the cell, given by the product of current and time. This implies that for the different current densities employed, the same amount of aluminium was oxidized (for 3*F* charge 1 mol is oxidized [1]). A charge density of 80 C dm^{-2} was selected, at which steady-state anodic oxide growth had been attained for all current densities, as revealed in the potential–time transients. Thus, anodizing at 0.8 A dm^{-2} was continued for 100 s, whereas, at 20 A dm^{-2}, anodizing proceeded for 4 s.

Figures 7, 8 and 9 display the oxide thickness across the diameter of the electrode for anodizing at 4, 8 and 20 A dm^{-2}, respectively. The flow condition clearly influences the film thickness distribution. In Figure 7, for the zero jet condition, the oxide thickness is greatest at the centre and decreases towards the rim of the electrode. For wall-jet flows 1 and 2, the film is thinner at the centre. Further, at 4 A dm^{-2}, the thickness profiles corresponded to the symmetrical rings of different appearance.

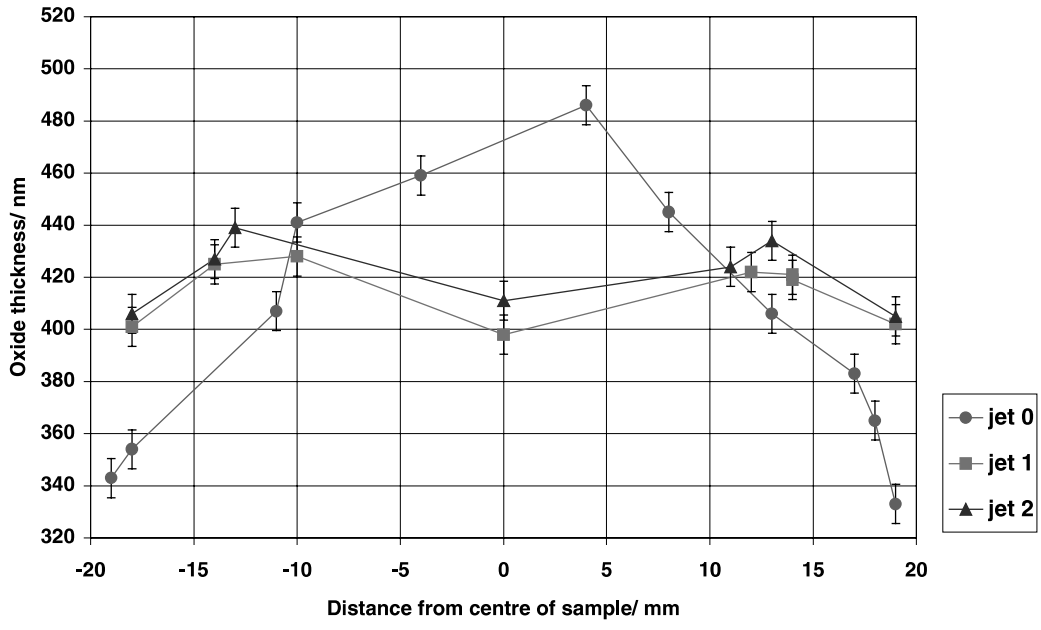

Fig. 7. Oxide thickness distribution for AA1050 Al anodized at 4 A dm^{-2} for 20 s in 20 wt % H_2SO_4 at 25 °C.

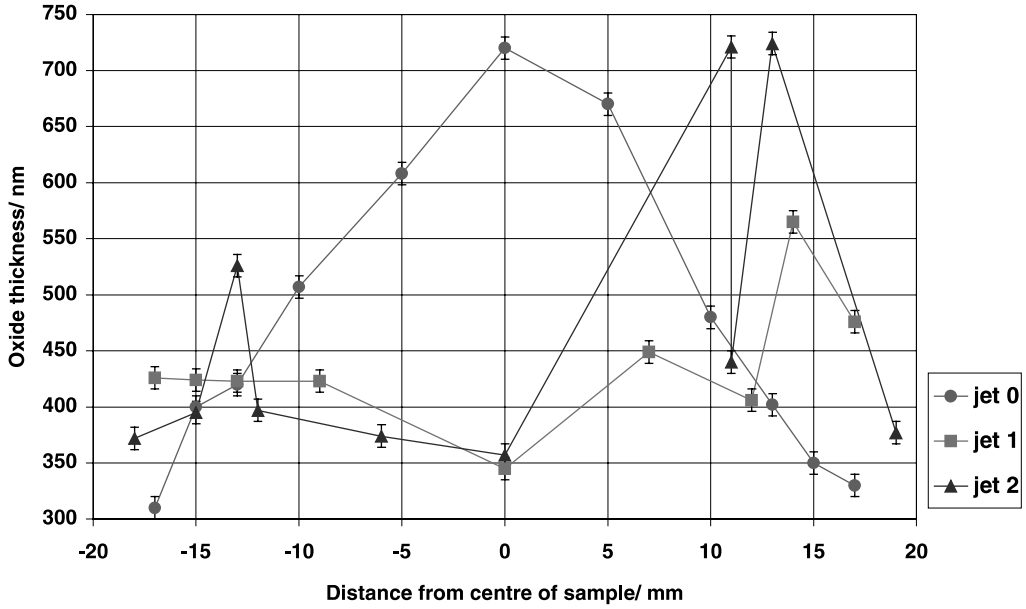

Fig. 8. Oxide thickness distribution for AA1050 Al anodized at 8 A dm^{-2} for 10 s in 20 wt % H_2SO_4 at 25 °C.

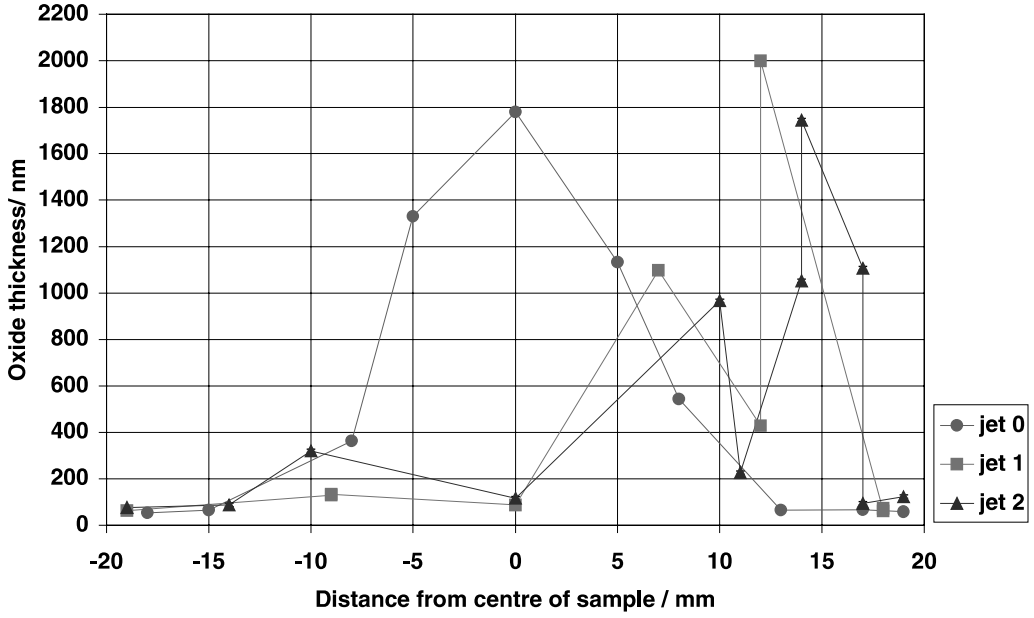

Fig. 9. Oxide thickness distribution for AA1050 Al anodized at 20 A dm^{-2} for 4 s in 20 wt % H_2SO_4 at 25 °C.

A local phenomenon occurred for anodizing at current densities of 8 A dm^{-2} and above, where a white spot appeared on the electrode. The spot is associated with a thicker oxide film than the surrounding regions. The position of the spot was independent of the relative position of the counter or reference electrode, thus eliminating possible geometrical asymmetry of the electrical current flow pattern. In Figure 9, the spot of thicker oxide film was at the centre of the electrode for the zero jet condition, and was located further away from the centre as the flow rate increased.

With continued anodizing at 20 A dm^{-2} for 4 min, a similarly shaped film thickness distribution was evident (Figure 10). The local white spot, with its associated thicker oxide film, remained apparent on the electrode surface.

3.4. *Influence of convection on the local electrode temperature*

The local electrode temperatures monitored during anodizing under the various conditions are shown in Figures 11 to 13. For all conditions, the electrode temperature increased; generally, the higher the current density the greater the temperature rise and rate of increase. This is consistent with the temperature increase

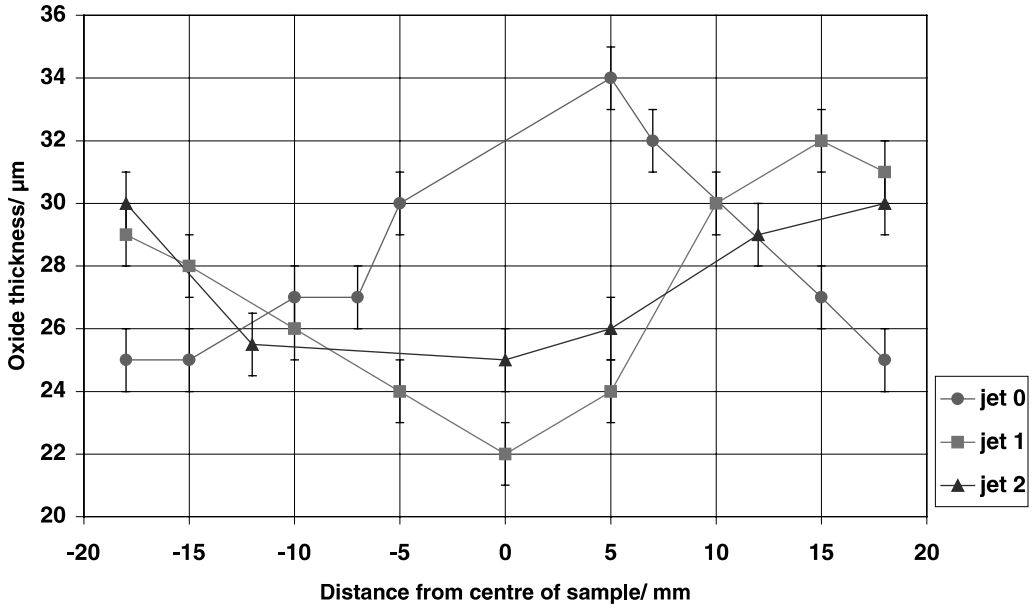

Fig. 10. Oxide thickness distribution for AA1050 Al anodized at 20 A dm^{-2} for 240 s in 20 wt % H_2SO_4 at 25 °C.

resulting largely from the dissipated electrical power in the electrode (i.e., Joule heating) which is proportional to the time dependent electrode resistance and the square of the current.

Comparing Figures 11 and 12, it is evident that the temperature rise decreases with increased electrolyte agitation. Further, the higher the electrolyte flow rate, the greater the overall heat transfer coefficient, as expected, and in agreement with the results for anodizing in phosphoric acid with and without stirring [23].

Figure 11 shows that at 8 A dm^{-2}, in the zero jet condition, the temperature was highest at the centre of the electrode (T3) and decreased gradually in the radial direction, confirming the natural convection flow pattern. For jet flows 1 and 2, the temperature distributions were inverted, which is illustrated in Figure 12 for jet flow 1. In this case, T3 registered the lowest temperature, due to impingement of fresh electrolyte from the nozzle, while the temperature increased towards the rim of the sample. The diametrically placed T1 and T5 registered similar temperature rises, confirming wall-jet symmetry.

For anodizing at 20 A dm^{-2}, under jet flow 1 (Figure 13), in the initial few seconds, thermocouple T5 recorded a peak value. Further, the temperature peak was always

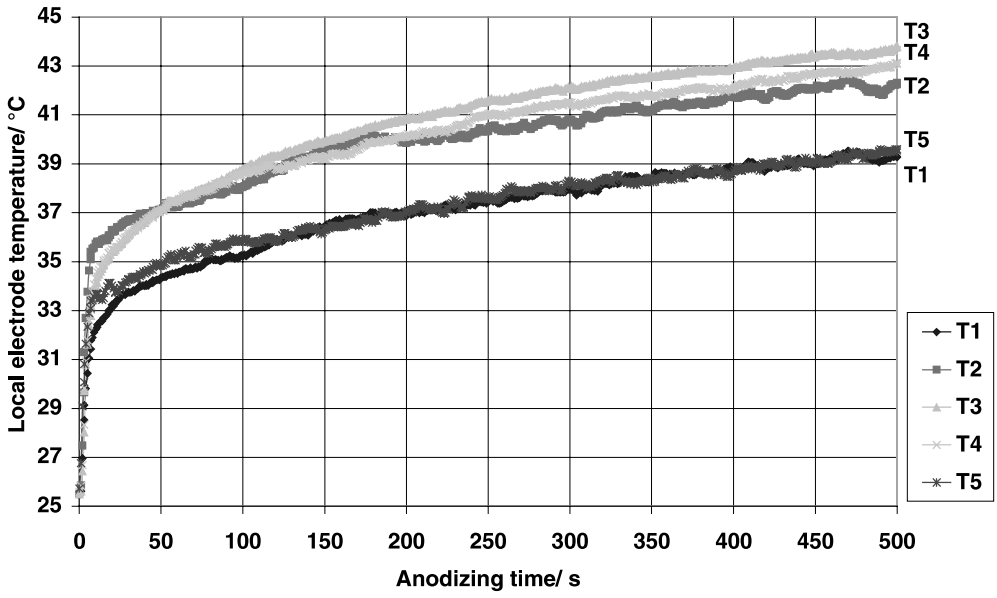

Fig. 11. Variation of local electrode temperature for anodizing at 8 A dm^{-2} in 20 wt % H_2SO_4 at 25 °C under zero jet condition.

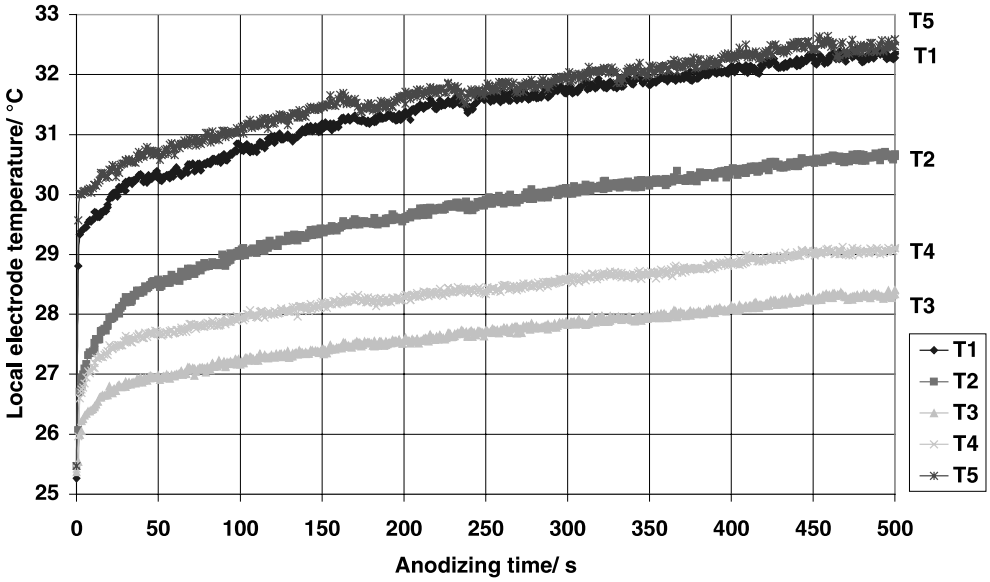

Fig. 12. Variation of local electrode temperature for anodizing at 8 A dm^{-2} in 20 wt % H_2SO_4 at 25 °C under jet flow condition 1.

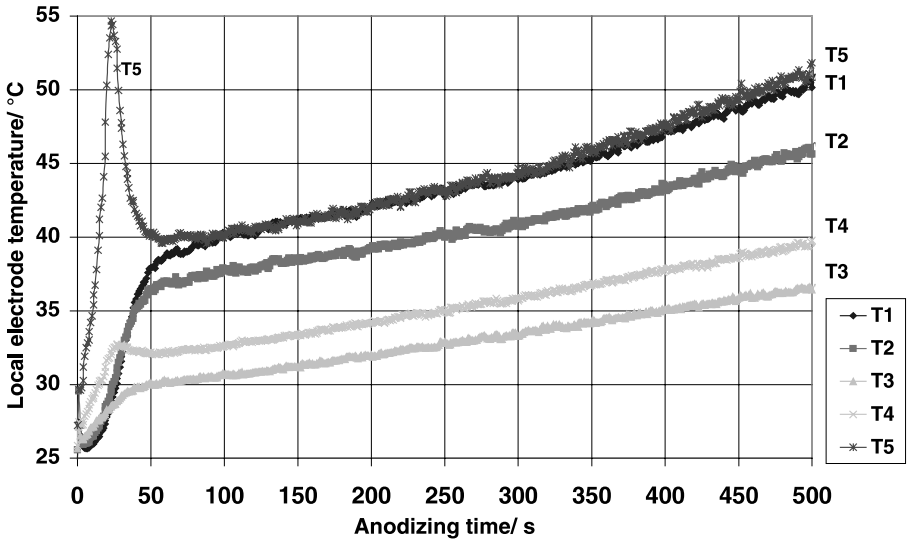

Fig. 13. Variation of local electrode temperature for anodizing at 20 A dm^{-2} in 20 wt % H_2SO_4 at 25 °C under jet flow condition 1.

registered by the thermocouple closest to the local white spot of thicker oxide on the sample, indicating its association with local heat generation.

4. Discussion

4.1. *General observations*

4.1.1. *Anodizing potential*

From the potential-time measurements, it is evident that for the zero jet condition, where the average electrode temperature is higher, the potential is lower than for jet flows 1 and 2. In other words, the higher the interfacial temperature, the lower the steady-state potential. The reduced steady-state potential is associated with an anodic film of decreased barrier layer thickness, as confirmed by transmission electron microscopy; the pore population density, or distribution of the alumina, also varies with anodizing voltage. The results also confirm that the field-assisted dissolution of the oxide is thermally enhanced [8, 14].

4.1.2. *Temperature variation with anodizing*

The trend of temperature rise with increase of current density is expected; thus an increased current leads to enhanced temperatures, and a higher jet flow rate acts to reduce the temperature increase. A steady temperature is however not readily achieved. This is due to the effect of thermal conduction to the sample holder superposed on the convection effect, delaying a steady temperature condition.

The most significant heat contribution is from Joule heating of the anodic oxide covered electrode. During

steady-state anodizing, the barrier thickness normally remains constant. Consequently, the Joule heat flux (W m^{-2}) should reach a steady value of Vi, where V is the anodizing potential (V) and i the current density (A m^{-2}).

The overall heat removal at steady-state is (mainly) determined by the jet flow rate. For the wall-jet hydrodynamic flow system, the dimensionless expression for the Nusselt number Nu, containing the overall convective heat transfer coefficient h_t, derived from the mass transfer limiting current density relationship [29], is given by Equation 1:

$$Nu = h_t a/k = 1.59\, k_r (a/R)^{5/4} Pr^{1/3} Re_a^{3/4} \quad (1)$$

where:

h_t = overall convective heat transfer coefficient (W m^{-2} K^{-1})
k_r = dimensionless reactor parameter (0.82 for employed wall-jet reactor [26])
a = jet nozzle diameter (m)
R = radius of the electrode (m)
V_f = volumetric jet flow rate (m^3 s^{-1})
k = thermal conductivity of the fluid (W m^{-1} K^{-1})
v = kinematic viscosity of the fluid (m^2 s^{-1})
α = $k/\rho C_p$ = diffusivity of the fluid (m^2 s^{-1})
ρ = density of the fluid (g m^{-3})
C_p = heat capacity of the fluid (J g^{-1} K^{-1})
Pr = Prandtl = V/α
Re_a = Reynolds number = $4V_f/(\pi\, a\, v)$.

The physical properties of the electrolyte (20 wt % H_2SO_4 at 25 °C) in Table 1 and the wall-jet reactor parameters in Table 2 were used for calculation of the dimensionless numbers Pr and Re_a and the overall heat transfer coefficients h_t (Table 3).

On the basis that Joule heating is removed by convection, Equation 2 can be used to estimate temperature rises:

$$Vi = h_t(T - T_{\text{bulk electrolyte}}) \quad (2)$$

For steady-state anodizing at 8 A dm^{-2} and jet flow 1 ($V = 18$ V), the calculated temperature of 27.5 °C is reasonably close to the measured temperatures of 27.0 °C at the centre of the electrode and 31.0 °C at the rim of the electrode (Figure 12). The latter are local temperatures, determined by the local heat transfer coefficients, explaining the deviation. Similar calculations for 20 A dm^{-2} and jet flow 1 ($V = 22$ V) yield a temperature of 33 °C, a value within the range of the local temperatures from 30.5 °C at the centre to 39.5 °C at the rim of the electrode.

Table 1. Physical properties of 20 wt % H_2SO_4 at 25 °C

k/W m^{-1} K^{-1}	0.46
v/m^2 s^{-1}	1.47×10^{-6}
ρ/g m^{-3}	1.136×10^{6}
C_p/J g^{-1} K^{-1}	3.53

Table 2. Wall-jet electrode reactor parameters

a/m	2×10^{-3}
R/m	2×10^{-2}
k_r	0.82
V_{f1}/m^3 s^{-1}	1.78×10^{-6}
V_{f2}/m^3 s^{-1}	3.48×10^{-6}

Table 3. Hydrodynamic parameters for the jet flow rates 1 and 2

	Pr	Re_a	h_t/W m^{-2} K^{-1}
Jet flow 1	12.8	770	5770
Jet flow 2	12.8	1507	9540

4.2. *Local observations*

Clearly, use of the wall-jet reactor enables variation of heat transfer over the electrode surface. Thus, the general observations of the previous Section relate to the compromise behaviour of the electrode. By considering the local behaviour, in particular, the variation of film thickness across the electrode, the variation of current flow over the planar electrode surface can be considered further.

The distribution of the oxide thickness is related to the temperature distribution which, in turn, is related to the local power employed, and consequent heat generation. In other words, the greater the local temperature the greater the field assisted dissolution and, hence, to maintain equilibrium, the greater the local growth rate of the porous anodic film. Although a constant current density flows through the cell, the local current requirements of the electrode will vary with temperature. Consequently, locally hotter regions will be associated with greater local currents. The effects of the local temperature rise on chemical dissolution of the generated porous anodic alumina film are largely ignored here since such effects are small compared with those of thermally enhanced field assisted dissolution.

The consequence of the previous is that the film thickness and the anodic film parameters are not uniform over the electrode surface. Further, the metal–film interface will also reveal local geometric change; greater recession of the metal–film interface will have proceeded in regions of increased local film thickness. Thus, the consequences of local temperature variation over the electrode surface are nonuniform current flow, nonuniform porous anodic alumina thickness and local alteration of the interfacial geometry.

4.3. *Nonuniform film formation*

In addition to electrode temperature variation, other features observed include local spots of thicker oxide generation, and secondary voltage rises at increased current densities of anodizing. Concerning the locally thicker oxide growth, this is associated with regions of initial transient temperature rise. The transient nature implies that the local phenomena proceeding are

quenched relatively rapidly; however, because of the initial high current flow, with a high rate of film growth and local metal–film interface alteration as results, the local region remains visible throughout the period of anodizing. As a partial explanation of the presence of such regions, flaw behaviour is considered. Thus, over the electrode surface, initially supporting an air-formed film, flaws are always present. The flaws are associated with regions of impurity and/or geometrical change. Generally during anodizing such flaws are healed by film growth. However, for the conditions of anodizing in the wall-jet reactor, with variation of heat transfer and, hence, local temperature over the electrode surface, it is possible that a particular flaw area into which current is focused results in a critical temperature generation. The temperature rise may initially influence the film conductivity to such an extent that further current is focused into the local region. This continues until the area and its zone of influence at the metal–film interface increases to a level where the local current density eventually declines and the processes contributing are quenched, enabling film growth to proceed in the usual manner. The previous reasoning can also explain the influence of the jet flow rate on the position of the spot of locally thick oxide. At high flow rates the heat transfer coefficient, allowing the temperature to reach a critical level at a flaw site, will be at a more eccentric position on the electrode surface.

With regard to the secondary voltage rises, it is generally regarded that the anodic film parameters respond directly to the voltage increase (i.e., the barrier layer thickness increases as the voltage increases). However, the precise thickness to voltage ratio is unavailable and hence, any change in field strength for ionic transport can not be considered further. Such voltage rises are associated with increased current densities and, interestingly, under conditions of increased heat transfer, the monitored voltage increases. Additionally, during the period of voltage rise, porous anodic film formation continues at relatively high rates. As with many facets of anodizing and associated ionic transport, precise reasons for this behaviour are awaited; factors considered previously have included anion depletion or cation accumulation in the pore base electrolyte or reduction in film conductivity (implying a local structural alteration). A factor countering the previous, at least partially, is the continued porous film growth during the anomalous period of anodizing. The results of the previous study also indicate that for conditions of enhanced mass transport (i.e., higher jet flow rate) the phenomenon is not enhanced, nor reduced, again implying that mass transport *per se* is not a controlling factor. Change in film conductivity, possibly through generation of nanocrystallinity within the barrier layer material, is also of potential interest; however, the cooperative processes of cation egress and anion ingress act generally to remove such film crystallinity. A further possibility is that a critical heat generation and its removal through convective heat transfer act to alter the local co-ordination of aluminium with oxygen in the newly generated barrier film material. Generally, a variation of coordination of Al^{3+} ions with O^{2-} ions is evident, including four-, five- and sixfold coordination. Thus, possibly, a move to a more symmetrical arrangement of aluminium and oxygen, i.e. the octahedral arrangement, in the amorphous barrier layer influences the dissolution of the film under the local field at the pore base. These and other phenomena require further scrutiny, which are possible under the condition of the wall-jet electrode.

5. Conclusions

It has been demonstrated that for the purpose of this type of investigation the wall-jet electrode system is a suitable tool. Convection can be introduced as a controlled parameter, and the inherent nonuniform heat transfer distribution of the wall-jet hydrodynamics allows the influence of local differences to be investigated.

Convective heat transfer has a significant influence on anodic oxide formation. Due to local temperature differences, a result of the nonuniform heat transfer distribution, a local current density distribution is established. The higher the local temperature, the higher the local current density and hence, the thicker the anodic film [35, 36].

The higher the current density the more pronounced the influences of heat transfer. Localized effects are evident; local temperature surges related to spots of thicker anodic alumina are observed. Secondary voltage rises arise after longer anodizing periods.

Acknowledgements

The authors acknowledge the support of Corus Aluminium (Duffel); we are especially grateful to E. Verboom for her support and interest and to B. Van der Linden for the discussion time. The Flemish Institute for the Advancement of Scientific – Technological Industrial Research (IWT) is acknowledged for funding. We are grateful to Alcan International Limited (Banbury) for the TEM measurements. At the University of Brussels (V.U.B.) we acknowledge M. Raes, M. Depauw and A. De Coninck for their valuable assistance.

References

1. S. Wernick, R. Pinner and P.G. Sheasby, 'The Surface Treatments and Finishing of Aluminium and its Alloys', Vol. 1, 5th, ASM international symposium, Ohio (1987).
2. Y. Xu, 'The Growth Mechanisms of Anodic films on Aluminium', PhD UMIST, GB (1983).
3. L. Young, 'Anodic Oxide Films' (Academic Press, London, 1961).
4. J.W. Diggle, 'Oxides and Oxide Films', Vol. 1, (Dekker, New York, 1973).
5. J. Siejka and C. Ortega, *J. Electrochem. Soc.* **124** (1977) 883.

6. J.F. Murphy and C.E. Michelson, *Proceedings of a conference on* '*Anodizing Aluminium*', *Aluminium Development Association*, Nottingham (1961), p. 83.
7. T.P. Hoar and M.F. Mott, *J. Phys. Chem. Solids* **9** (1959) 97.
8. J.P. O'Sullivan and G.C. Wood, *Proc. Roy. Soc. Lond. A* **317** (1970) 511.
9. J.P. O'Sullivan and G.C. Wood, *Electrochem. Acta* **15** (1970) 1865.
10. M. Nagayama and K. Tamura, *Electrochem. Acta* **13** (1968) 1773.
11. N. Sato, *Electrochem. Acta* **16** (1971) 1683.
12. W.E. Cooke, *Plating* **62** (1975) 239.
13. J.M. Kape, *Met. Fin. J.*, Apr. (1974).
14. G.C. Tu, 'The Growth of Porous Anodic Films on Aluminium under DC and AC Conditions', PhD, UMIST, GB (1981).
15. N. Klein, *in* L. Marton (Ed.), 'Electrical Breakdown in Solids', (Adv. Electr. Electron Physics), Vol. 26, (Academic Press., New York, 1969).
16. D.A. Vermilyea, *Acta. Metall.* **1** (1953) 282.
17. L. Young, *Trans. Farad. Soc.* **53** (1957) 229.
18. M.S. Hunter and P. Fowle, *J. Electrochem. Soc.* **101** (1954) 481.
19. M. Nagayama and K. Tamura, *Electrochem. Acta* **13** (1968) 1773.
20. R.B. Mason, *J. Electrochem. Soc.* **102** (1955) 671.
21. F.R. Applewhite, J.S.L. Leach and P. Neufeld, *Corros. Sci.* **9** (1969) 305.
22. I. Mizuki, N. Baba and S. Tajima, *J. Met. Finish. Soc. Jpn.* **28** (1977) 30.
23. S. Pierrard, 'Rapid Anodic Film Growth on Aluminium, PhD, UMIST, GB (1987).
24. S. Pierrard, G.E. Thompson, M. Badia and G.C. Wood, *Trans. IMF* **66** (1988) 122.
25. T. Imamura, S. Hoshino and S. Matsumoto, *J. Met. Finish. Soc. Jpn.* **28** (1977) 22.
26. P. Laevers, A. Hubin, H. Terryn and J. Vereecken, *J. Appl. Electrochem.* **3** (1995) 1017.
27. P. Laevers, A. Hubin, H. Terryn and J. Vereecken, *J. Appl. Electrochem.* **3** (1995) 1023.
28. P. Laevers, A. Hubin, H. Terryn and J. Vereecken, *J. Appl. Electrochem.* **28** (1998) 387.
29. W.J. Albery, *in* R.G. Compton (Ed.), 'Comprehensive Chemical Kinetics', Vol. 29, (Elsevier, Amsterdam, 1989).
30. R. Gardon and J.C. Akfirat, *J. Heat Transf.* Feb. (1966) 101.
31. D.J. Bizzak and M.K. Chyu, *Int. J. Heat Mass Transf.* **38** (2) (1995) 267.
32. B. Elison and B.W. Webb, *Int. J. Heat Mass Transf.* **37** (8) (1994) 1207.
33. E. Cuynen, J. De Laet, H. Terryn and P. Van Espen, Proc. ECASIA95, 6th European conference on 'Applications of Surface and Interface Analysis' (1996) p. 851.
34. J. De Laet, H. Terryn, G.E. Thompson, B. Van Mele and J. Vereecken, Proc. 7th International symposium on 'Oxide Films on Metals and Alloys', *Electrochem. Soc., Proc. Vol.* **94-25** (1994), p. 13.
35. I. De Graeve, H. Terryn and E. Verboom, Proc. ASST II, *Aluminium Surface Science and Technology Conference II* (2000), p. 47.
36. A.J. Bosch, P. Boerstoel, Th. Zuidwijk, A. Hovestad, A. Plomp and J.A. van de Heuvel, Proc. ASST II, *op. cit.* [35], p. 65.